Evidence That Azide Occupies the Chloride Binding Site near the Manganese Cluster in Photosystem II †

ARTICLE *in* BIOCHEMISTRY · OCTOBER 2005

Impact Factor: 3.02 · DOI: 10.1021/bi0505767 · Source: PubMed

4 AUTHORS, INCLUDING:

Xianzhong Xu
University of Georgia
16 PUBLICATIONS **195** CITATIONS

SEE PROFILE

Evidence That Azide Occupies the Chloride Binding Site near the Manganese Cluster in Photosystem II†

Hui Yu, Constantino P. Aznar, Xianzhong Xu, and R. David Britt*

Department of Chemistry, University of California, Davis, California 95616-0935

Received March 29, 2005; Revised Manuscript Received July 1, 2005

ABSTRACT: The effect of adding azide to photosystem II (PS II) membrane samples (BBY preparation), with or without chloride, has been investigated using continuous wave (CW) and pulsed EPR spectroscopy. In the BBY samples with 25 mM chloride, we observed that the inhibition induced by azide is partly recovered by the addition of bicarbonate. Electron spin−echo envelope modulation (ESEEM) was used to search for spin transitions of ^{15}N nuclei magnetically coupled to the S_2 state Mn cluster (multiline EPR signal form) in ^{15}N (single terminal label) azide-treated samples with negative results. However, an ^{15}N ESEEM peak was observed in parallel chloride-depleted PS II samples when the ^{15}N-labeled azide is added. However, this peak is absent in chloride-depleted samples incubated in buffer containing both chloride and [^{15}N]azide. Thus these results demonstrate an azide binding site in the immediate vicinity of the Mn cluster, and since this site appears to be competitive with chloride, these results provide further evidence that chloride is bound proximal to the Mn cluster as well. Discussion on the possible interplay between azide, chloride, and bicarbonate is provided.

Photosystem II (PS II)[1] is a multisubunit chlorophyll−protein complex that uses light energy to oxidize water and form molecular oxygen, with a concomitant reduction of plastoquinone to plastoquinol (*1*, *2*). The catalytic center for the oxidation of two water molecules to one dioxygen molecule is composed of a spin-coupled tetramanganese cluster along with Ca^{2+} and Cl^- cofactors (*3*−*8*). A nearby redox-active tyrosine (Y_Z) serves as an electron transfer intermediate between the photooxidized $P680^+$ Chl and the Mn cluster, and it has been proposed to also couple proton transfer to this electron transfer (*9*, *10*).

The removal of calcium or chloride through dialysis of PS II samples against Ca^{2+}-free or Cl^--free buffers inhibits the advancement of the S-state cycle beyond S_2 (although one more donor side electron can be removed by trapping Y_Z in its oxidized neutral radical form $Y_Z^{\bullet}$) (*4*, *11*−*19*). Inhibition of oxygen evolution has also been observed when PS II is treated with nitric oxide or some weak anions such as azide, acetate, and nitrite, although the inhibition mechanism is still poorly understood (*16*, *20*−*25*). A previous ESEEM study showed that acetate binds to or near the Mn cluster and displaces water, which may directly relate to acetate's inhibitory effect (*14*, *26*). This raises the question as to whether other anions such as azide bind and inhibit in an analogous fashion.

It has been observed that bicarbonate can relieve to some extent the PS II inhibition induced by monovalent anions such as F^-, HCO_2^-, NO_2^-, NO_3^-, and Ac^- (*21*−*23*). However, N_3^- is an exception. Stemler et al. hypothesized that the azide anion binds to PS II at a site other than the HCO_3^- binding site (*21*). Recently, it has been suggested that azide inhibits oxygen evolution as a chloride competitor and that it prevents the OEC from undergoing the normal progression to the S_2 state (*24*, *25*).

In this work, we employ continuous wave (CW) and pulsed EPR to further investigate the effect of azide at various concentrations on PS II-enriched membrane preparations (BBY) (*27*), both in the presence and in the absence of chloride. We discuss the possibility that azide disrupts the normal proton-relay network and delays the release of protons from the water-splitting reaction.

MATERIALS AND METHODS

Materials. NaN_3 (99% ^{15}N single terminal labeled, $^{15}N^{14}N^{14}N^-$) was used as received from Cambridge Isotope Laboratories. All other chemicals were used as received from Fisher Scientific or Sigma.

Sample Preparation. PS II-enriched "BBY" membranes were prepared from spinach on the basis of the procedure developed by Berthold et al. (*27*, *28*), with some modifications provided by Campbell et al. (*29*). All steps were performed under dim green light or darkness in a cold room. Isolated BBY samples were resuspended in SMNCE buffer, which contains 400 mM sucrose, 20 mM MES−NaOH (pH 6.0), 15 mM NaCl, 5 mM $MgCl_2$, 5 mM $CaCl_2$, and 1 mM EDTA, and were then stored in liquid nitrogen until use. Protein analysis by SDS−urea−PAGE used a gel containing 6.0 M urea as described previously (*30*). The polyacrylamide concentrations of the stacking and separation gels were 4%

† We gratefully acknowledge the National Institute of Health (Grant GM 48242) for supporting this work.

* To whom correspondence should be addressed. Phone: (530) 752-6377. Fax: (530) 752-8995. E-mail: rdbritt@ucdavis.edu.

[1] Abbreviations: BBY, PS II-enriched thylakoid membrane; Chl, chlorophyll; CW, continuous wave; ENDOR, electron nuclear double resonance; EPR, electron paramagnetic resonance; ESE, electron spin−echo; ESEEM, electron spin−echo envelope modulation; EXAFS, extended X-ray absorption fine structure; OEC, oxygen evolution complex; PS II, photosystem II.

10.1021/bi0505767 CCC: $30.25
Published on Web 08/19/2005

and 15%, respectively. The gels were stained with Coomassie Brilliant blue R-250. Chl concentration and Chl *a*/*b* ratios were determined by Arnon's method (*31*).

Treatment with Azide of BBY Samples in the Presence of Chloride. BBY samples treated with NaN_3 (natural abundance or ^{15}N single terminal labeled) in the presence of 25 mM chloride were prepared as described in ref *25*. BBY samples were washed twice with a buffer containing 400 mM sucrose, 15 mM NaCl, 5 mM $MgCl_2$, and 20 mM MES−NaOH (pH 6.0) and then suspended to 0.5 mg of Chl mL^{-1} with the same buffer and varied concentrations of NaN_3. After incubation on ice for 30 min, BBY samples were centrifuged at 30000*g* for 30 min, and the resultant pellets were loaded into EPR tubes. For the experiments on bicarbonate effects on the BBY samples treated by azide, BBY samples treated by azide were reincubated in the same buffer (25 mM chloride) with additional $NaHCO_3$ for 30 min in a cold room (4 °C). After incubation on ice in the dark for about 30 min, all BBY samples were centrifuged at 30000*g* for 30 min. The final pellets were loaded into precision 3.8 mm o.d. quartz EPR tubes at final chlorophyll concentrations of 11−20 mg of Chl mL^{-1} and stored in liquid nitrogen until use.

Treatment with Azide of BBY Samples in the Absence of Chloride. BBY samples were depleted with chloride and treated with azide (natural abundance or ^{15}N terminal labeled) as follows (*25*, *32*): BBY samples were dialyzed in the dark at cold room temperature (4 °C) for 16−18 h against Cl^--free 20 mM MES−NaOH buffer, pH 6.3, with glycerol, 146.7 g L^{-1} (1.4 M). These BBY samples will be referred to as Cl^--depleted BBY samples in the following. After centrifugation, the pellets prepared from the dialyzed BBY samples were resuspended and diluted to about 0.3 mg of Chl mL^{-1} in a Cl^--free buffer (400 mM sucrose, 20 mM Mes−NaOH, pH 6.3) with NaN_3 of desired concentrations (natural abundance or ^{15}N terminal labeled). To investigate if azide is a competitor of chloride, a set of dialyzed BBY samples were treated with both NaN_3 (natural abundance or ^{15}N labeled) and 10 mM NaCl. Dark incubation, centrifuge pelleting, and EPR tube loading were performed as described above.

Sample Illumination. All samples were advanced to the S_2 state by illumination in a non-silvered dewar for 5 min at 195 K (dry ice/methanol). Illumination was performed with a focused Radiac light source. Samples were frozen immediately in liquid nitrogen within 2 s of illumination.

EPR Spectroscopy. CW-EPR spectra were recorded at a temperature of 7 K with a Bruker ECS 106 X-band CW-EPR spectrometer equipped with an Oxford ESR 900 liquid helium cryostat and an ITC 530 temperature controller. Electron spin−echo (ESE) field sweeps and ESE envelope modulation (ESEEM) spectra were collected at 4.2 K using an X-band laboratory-built pulsed EPR spectrometer (*33*). Two-pulse ESEEM experiments were performed by incrementing the time τ in the spin−echo sequence: $\pi/2-\tau-\pi-\tau-$echo. Time-domain ESEEM spectra were collected for both dark and illuminated samples. The "dark" spectra were subtracted from the "light" spectra to produce the "light minus dark" time-domain modulation patterns. A cosine Fourier backfill was used to reconstruct the dead time data needed to generate the final displayed cosine Fourier transfor spectra (*34*−*37*). Two-pulse ESEEM simulations were performed for the electron spin $S = {}^1/_2$ and nuclear spin $I = {}^1/_2$ using the analytical solution derived by Mims (*37*). For the $S = {}^1/_2$ and $I = 1$ case, ESEEM simulations were performed using the matrix diagonalization procedure as described previously (*35*).

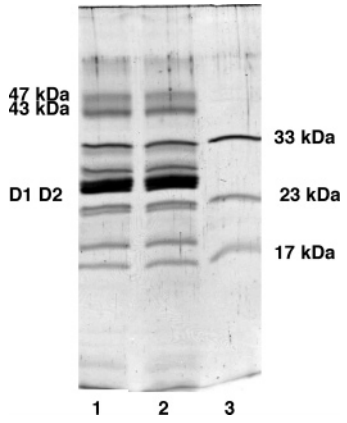

FIGURE 1: Electrophoretic pattern of isolated PS II-enriched membranes (BBY) in a 15% acrylamide gel containing 6 M urea. Numbers below the lane indicate (1) BBY control, (2) BBY membranes depleted of Cl^- by dialysis for 16 h against Cl^--free 20 mM MES−NaOH, pH 6.3, and 1.4 M glycerol buffer, and (3) the 17, 23, and 33 kDa extrinsic proteins (obtained from the supernatant of a urea-treated BBY sample).

RESULTS

Polypeptide Composition of BBY Samples and Cl^--Depleted BBY Samples. The polypeptide composition of extracted BBY samples as analyzed by SDS−urea−PAGE is shown in Figure 1. The gel pattern of the control sample (lane 1) shows several major polypeptides, including D1, D2, CP47, CP43, three extrinsic proteins, etc. After dialysis of a BBY sample against a Cl^--free medium containing glycerol, no change in polypeptide composition (lane 2) was observed compared to the control. Lane 3 shows the gel patterns of the 17, 23, and 33 kDa extrinsic proteins (*38*).

Inhibition Induced by Varied Concentrations of Azide for BBY Samples in the Presence of 25 mM Chloride. (A) CW-EPR Spectroscopy. It was previously reported that azide irreversibly inhibits oxygen evolution (*39*). Haddy et al. reported that NaN_3 at millimolar concentration suppresses the S_2 state signals of BBY samples in the presence of 25 mM chloride (*25*). In the experiment reported here, treatment of PS II samples in the presence of 25 mM Cl^- with varied azide concentrations (from 8 to 100 mM) suppressed both the $g = 2$ multiline signal and the $g = 4.1$ signal (Figure 2A). The S_2 state multiline EPR signal arises from a ground spin $S = {}^1/_2$ state of the antiferromagnetically exchange-coupled Mn cluster, while the $g = 4.1$ signal arises from a higher spin state (*40*, *41*). The suppressed EPR signal intensities induced by azide in these experiments suggest that azide could inhibit the donor side reaction of PS II through a weak binding to some sites in or near the OEC. In addition, Figure 2 also shows that the $g = 2$ multiline signal appeared to be more sensitive to azide than the $g = 4.1$ signal (Figure 2B). It was reported that binding of formate stimulates the EPR signal at $g = 1.82$ that arises from the light-induced $Q_A^-Fe^{2+}$ state of the PS II electron acceptor side (*42*, *44*; Yu, Britt, et al., unpublished results). As the concentration of azide was increased, however, the effect of azide on this

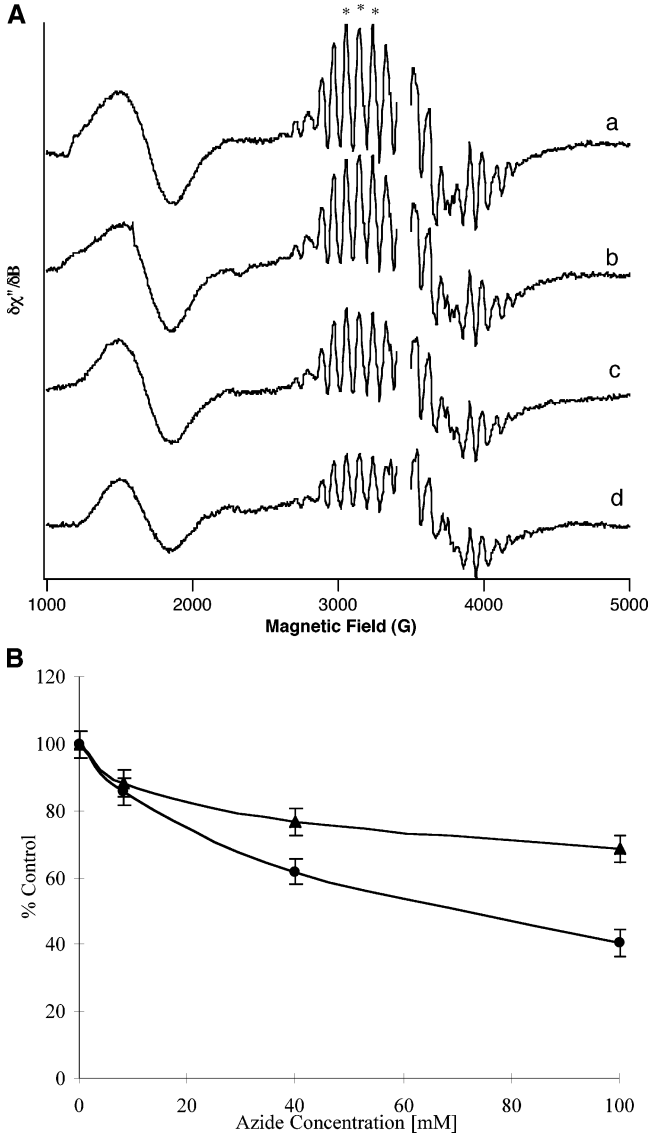

FIGURE 2: (A) CW-EPR spectra of BBY samples treated with varied concentrations of NaN_3: (a) 0 mM; (b) 8 mM; (c) 40 mM; (d) 100 mM. PS II samples were prepared in the presence of 25 mM Cl^-. Experimental parameters: microwave frequency = 9.68 GHz; microwave power = 5 mW; modulation amplitude = 9.74 G; modulation frequency = 50 kHz; temperature = 7 K. The averaged peak to peak heights of the features marked with asterisks were used to report the signal intensity of the $g = 2$ signal. (B) Azide concentration dependence of the intensities of the S_2 state CW-EPR signals: (●) $g = 2$ signal; (▲) $g = 4.1$ signal.

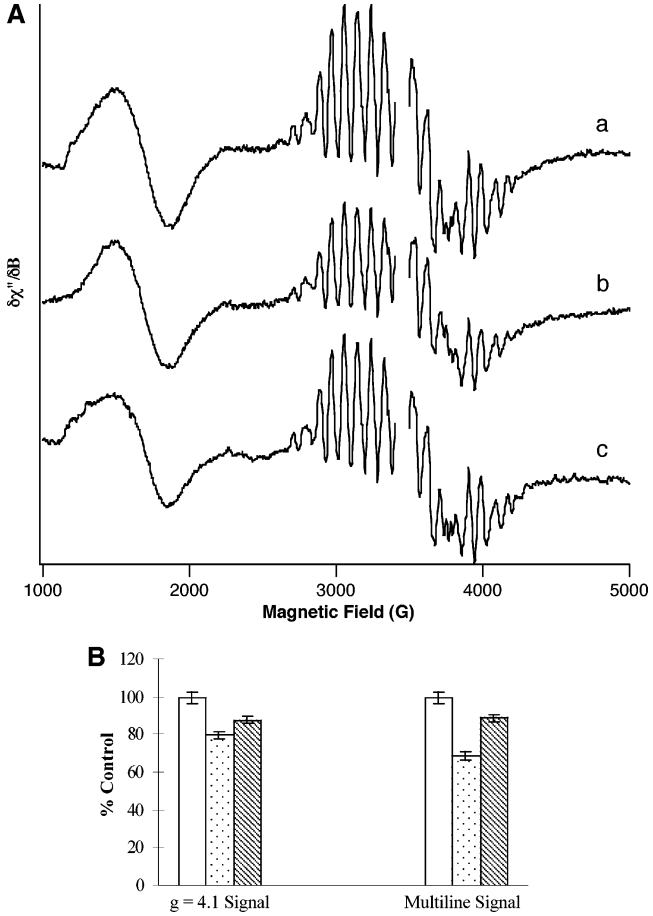

FIGURE 3: (A) CW-EPR spectra of (a) control (BBY), (b) 40 mM NaN_3-treated BBY sample, and (c) BBY sample treated previously with 40 mM NaN_3 with 10 mM bicarbonate subsequently added. All PS II samples were prepared in the presence of 25 mM Cl^-. Experimental parameters are as given in Figure 2. (B) Graphical summary of these EPR spectra. Bars: white, control; dots, 40 mM azide-treated BBY samples; right slashes, BBY samples treated previously with 40 mM azide with 10 mM bicarbonate subsequently added. The bar heights report averages of two to three independent spectral data sets.

acceptor side EPR signal seemed insignificant, quite different from the effect of formate, suggesting the absence of an analogous acceptor side binding site for azide.

It was observed that bicarbonate could relieve to some extent the inhibitory effect induced by monovalent anions such as formate on PS II (*21*−*23*). As mentioned in the introduction, however, Stemler et al. observed that the inhibitory effect of azide on PS II cannot be relieved by HCO_3^-. Only at high concentration (higher than 20 mM), or in the light, will N_3^- effectively compete with HCO_3^- (*21*). Haddy et al. also reported that azide inhibition is not relieved by bicarbonate (*24*), though removing azide by washing azide-treated PS II samples with azide-free buffer partly recovers the amplitude of the S_2 state EPR signals (*24*). In the experiments reported here, we observed that the inhibition of S_2 state EPR signal intensity (by 31% for the $g = 2$ multiline signal and 20% for the $g = 4.1$ signal) induced by 40 mM NaN_3 (natural abundance, [^{14}N]azide) in the presence of 25 mM Cl^- could be partly reversed by the addition of 10 mM bicarbonate. The sample containing bicarbonate showed $g = 4.1$ and $g = 2$ signal intensities of about 88% and 89%, respectively, vs controls [panels A (c) and B of Figure 3].

(B) Pulsed EPR Spectroscopy. Figures 4−6 show pulsed EPR results for BBY samples containing 25 mM Cl^-. Figure 4 shows the field-swept ESE spectra of the dark-adapted samples (labeled as dark) and illuminated samples (labeled as light), as well as the difference spectra isolating the S_2 state signal (labeled as light minus dark). Figure 4A shows the spectra of the control BBY sample. Panels B and C of Figure 4 display those of the NaN_3-treated BBY samples, natural abundance (B) and ^{15}N terminal labeled (C). The line shapes of the three different spectra are essentially the same (Figure 4). Figure 5 shows the various time-domain two-pulse ESEEM spectra measured at a static field of 3430 G (see Figure 4). Again, data were recorded before (dotted lines) and after illumination (dashed lines). The difference (solid lines) spectra show the modulation of the light-induced multiline EPR signal resulting from magnetic nuclei coupled

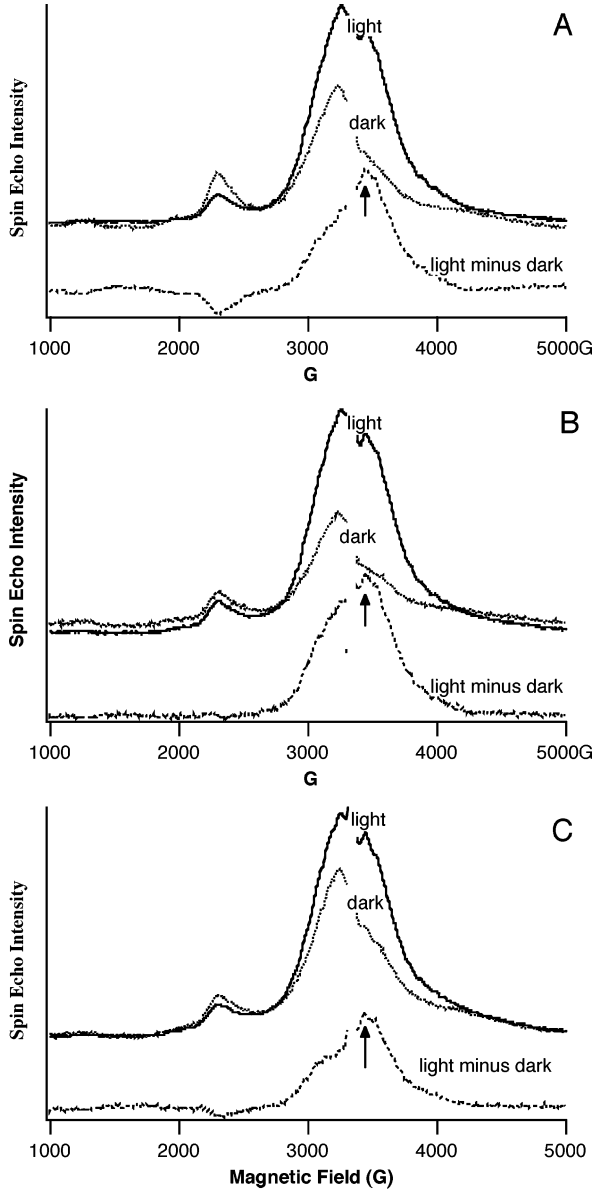

FIGURE 4: ESE field-swept spectra of BBY PS II samples prepared in the presence of 25 mM Cl^-. Panels: (A) control; (B) with 8 mM natural abundance NaN_3; (C) with 8 mM ^{15}N terminally labeled NaN_3. Panels A−C show the ESE field-swept EPR spectra of samples prior to illumination (dark traces), after illumination (light traces), and the difference spectra (traces light minus dark). Experimental parameters: microwave frequency = 9.339 GHz; microwave power = 20 W; repetition rate = 200 Hz; τ = 210 ns; $\pi/2$ pulse length = 11 ns; temperature = 4.2 K. Arrows indicate the magnetic field used to collect the ESEEM spectra shown in Figure 5.

to the Mn cluster. Figure 6 shows the Fourier transform (frequency-domain) spectra of the normalized difference ESEEM traces (Figure 5, solid lines). The 14.6 MHz peak is from coupled protons, and the broad peak centered at 4.8 MHz arises from a histidine [^{14}N]nitrogen (*35*). The control sample and the two different azide nitrogen isotope samples showed the same ESEEM spectra within our typical experimental reproducibility. Therefore, these experiments provided no positive indication of azide binding close to the Mn cluster in the presence of 25 mM Cl^-.

Inhibition Induced by Varied Concentrations of Azide for BBY Samples in the Absence of Chloride. (A) CW-EPR Spectroscopy. Figure 7b shows the S_2 state CW-EPR spectrum of a Cl^--depleted PS II sample, with significantly lower signal amplitude than the control sample (Figure 7a). We observed that the addition of 10 mM chloride to the Cl^--depleted PS II sample (on ice in darkness with 30 min incubation) almost fully rescued the $g = 2$ multiline signal but provided less recovery of the $g = 4.1$ signal (Figure 7c), consistent with a previous report (*32*). Treating a Cl^--depleted BBY sample with 8 mM azide partly recovered both $g = 2$ and $g = 4.1$ S_2 EPR signals (Figure 7d). However, incubation of a Cl^--depleted PS II sample with both 10 mM Cl^- and 8 mM azide resulted in a depressed $g = 4.1$ signal compared to the $g = 2$ multiline signal (Figure 7e), showing that at these relative concentrations the added chloride manifests a stronger influence on the OEC spin state than does azide.

(B) Pulsed EPR Spectroscopy. ESE field-swept spectra of Cl^--depleted and azide-repleted BBY samples (not shown) are analogous to those shown in Figure 4. Figure 8 shows the FT of the time-domain ESEEM (not shown) for selected repleted samples. Figure 8, trace a, compares the ESEEM of the Cl^--depleted ^{15}N terminally labeled azide-repleted sample to that of a control. A strong new peak is observed at about 1.9 MHz (which is 0.4 MHz higher than the 1.5 MHz ^{15}N Larmor frequency). This feature was reproduced in three independent preparations, with a frequency of 1.82 ± 0.08 MHz. No such peak was observed using ^{15}N-labeled azide when repleted along with chloride (Figure 8c). As previously noted, the ESEEM obtained using ^{15}N-labeled azide in a non-chloride-depleted sample is identical to that of a control sample (Figure 6). Contrasting the spectrum of the ^{15}N terminally labeled azide sample with that using natural abundance azide (Figure 8b) shows that the 1.9 MHz ESEEM feature arises from the terminal azide ^{15}N label. The spectra of Figure 8, traces b and c, lacking a 1.9 MHz peak, were also reproduced in three preparations. The clear conclusion arising from these ESEEM experiments is that azide binds in close proximity to the Mn cluster in the S_2 state in the absence of chloride. Given that the illumination to advance from the S_1 to the S_2 state was done at the low 195 K temperature, it is likely that azide is also bound at the S_1 state as well.

The upshift of the 1.9 MHz ^{15}N peak compared to the 1.5 MHz ^{15}N Larmor frequency indicates a nonzero isotropic coupling to the labeled azide terminus. Figure 9 shows two-pulse ESEEM FFT simulations for both the ^{15}N and ^{14}N (natural abundance) samples. To match the relaxation-induced phase memory decay of the experimental data, each simulated time-domain spectrum was multiplied by an exponential damping function (damping time = 0.9 μs) before the Fourier transformation. The 1.9 MHz ^{15}N peak frequency was well reproduced in a simulation using an isotropic ^{15}N hyperfine coupling of 0.70 MHz (along with a 0.3 MHz dipolar coupling). One would expect a matching lower frequency transition (~1.1 MHz) for the $I = {}^1/_2$ ^{15}N nucleus (see vertical lines in Figure 9), and this was indeed observed in the undamped simulation (not shown), but this lower frequency peak, corresponding to a longer period time-domain oscillation, was largely suppressed when the damping function was applied to simulate the phase memory decay of the experimental spectrum. In addition, the two-pulse ESEEM simulation shows the expected out-of-phase transition at the "sum" frequency of 3.0 MHz. This negative peak

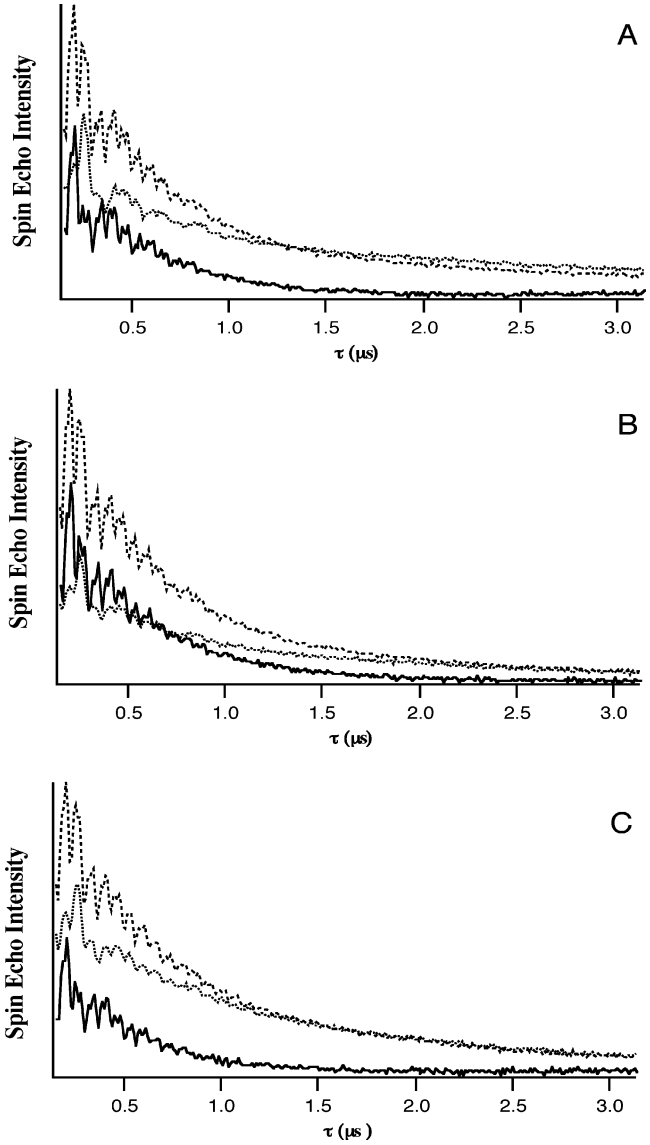

FIGURE 5: Two-pulse time-domain ESEEM spectra of BBY PS II samples prepared in the presence of 25 mM Cl^-. Panels: (A) control; (B) with 8 mM natural abundance NaN_3; (C) with 8 mM ^{15}N terminally labeled NaN_3. Shown are the ESEEM patterns of the samples prior to illumination (dotted traces), after illumination (dashed traces), and the light minus dark difference spectra (solid traces). Experimental parameters: microwave frequency = 9.339 GHz; B = 3430 G; starting τ = 180 ns; τ increment = 10 ns; microwave power = 20 W; repetition rate = 200 Hz; $\pi/2$ pulse length = 11 ns; π pulse length = 23 ns; temperature = 4.2 K.

seems to be observed in the experimental spectrum (compare the [^{15}N]- and [^{14}N]azide spectra, for example), but its assignment is not completely clear as this frequency overlaps with the lower frequency edge of the broad histidine peak. Our simulations also reproduced the lack of observed ^{14}N modulation in the natural abundance azide spectrum. The ^{14}N simulation used the same hyperfine tensor as for the ^{15}N case, scaled by the respective magnetogyric ratios, but included a nonzero nuclear quadrupolar interaction (nqi) for the $I = 1$ ^{14}N nucleus. A ^{14}N eeqQ value of 2.0 MHz (η = 0) was chosen on the basis of an azide solution NMR study (*44*, *45*). For the modest isotropic coupling employed here (lower than the "exact cancellation" matching condition that gives favorable ^{14}N modulation) (*46*), the effect of the nonzero nqi is to broaden and decrease the amplitude of the

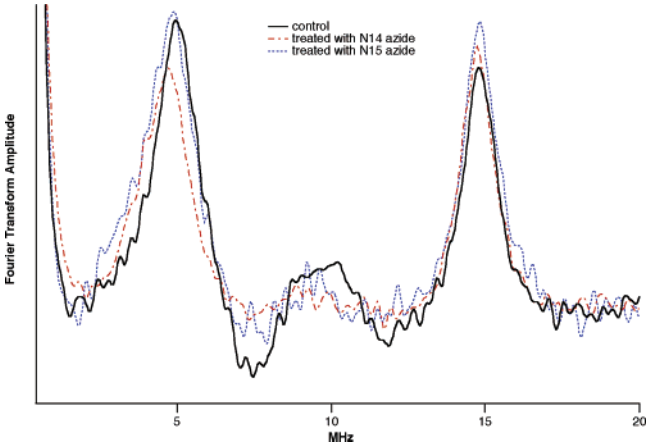

FIGURE 6: Fourier transform spectra of the light minus dark two-pulse ESEEM time-domain spectra of Figure 5: control, solid trace; 8 mM natural abundance NaN_3, dashed trace; 8 mM ^{15}N terminally labeled NaN_3, dotted trace.

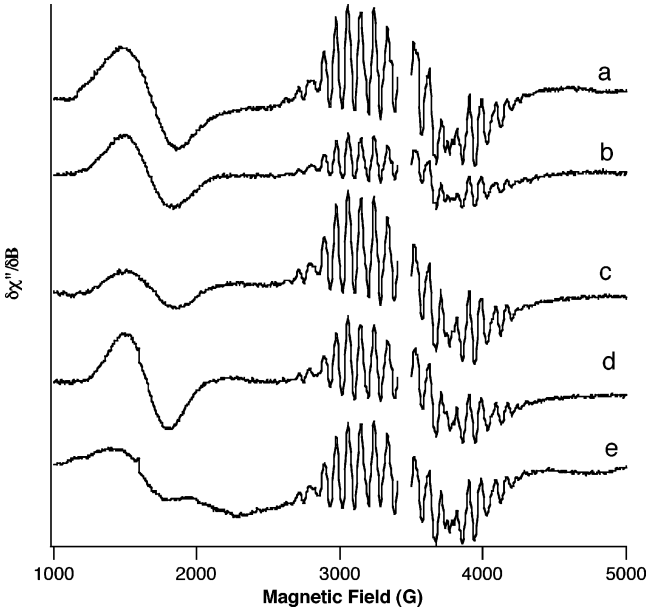

FIGURE 7: CW-EPR spectra of Cl^--depleted BBY samples repleted with various anions: (a) control (BBY); (b) Cl^- depleted; (c) 10 mM NaCl; (d) 8 mM NaN_3; (e) 8 mM NaN_3 plus 10 mM NaCl. PS II samples were prepared in the absence of Cl^-. Experimental parameters are as given in Figure 2.

^{14}N peaks (*47*). Peaks were observed in the undamped simulation (not shown), but after the exponential damping function was applied, the simulated frequency-domain spectrum was quite featureless, matching the experimental observation.

DISCUSSION

Azide was found to be an inhibitor of oxygen evolution of PS II in previous studies (*20*−*25*, *39*). However, the inhibitory mechanism of azide on oxygen evolution of PS II remains unclear. In the presence of 25 mM chloride, we show that azide can suppress both S_2 state CW-EPR signals, and the $g = 2$ multiline signal appears to be more sensitive to azide than the $g = 4.1$ signal (Figure 2). These results suggest that azide might inhibit water oxidation on the donor side of PS II. We do not find a significant azide effect on the light-induced $Q_A^-Fe^{2+}$ signal at $g = 1.82$ under our experimental condition, which could be taken as additional

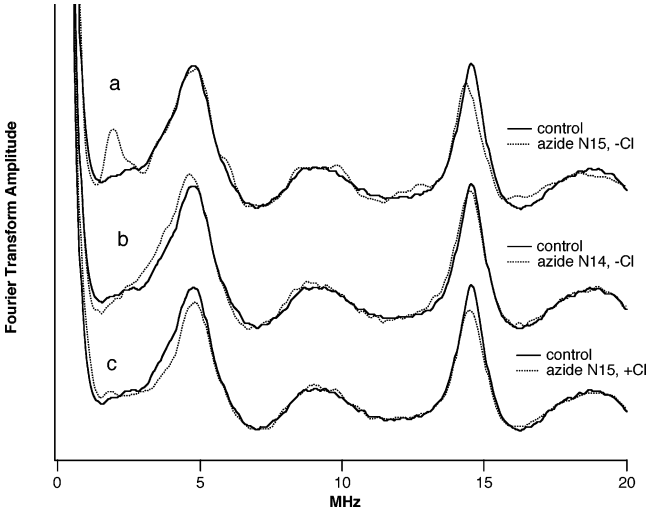

FIGURE 8: Fourier transforms of the light minus dark two-pulse ESEEM time-domain spectra obtained from Cl^--depleted BBY samples repleted with various anions (dotted traces) and compared with BBY controls (solid traces): (a) 8 mM ^{15}N-terminally labeled azide; (b) 8 mM natural abundance azide; (c) 8 mM ^{15}N-terminally labeled azide plus 10 mM NaCl. Experimental parameters: microwave frequency = 9.315 GHz; B = 3418 G; starting τ = 180 ns; τ increment = 10 ns; microwave power = 20 W; repetition rate = 200 Hz; $\pi/2$ pulse length = 11 ns; π pulse length = 23 ns; temperature = 4.2 K.

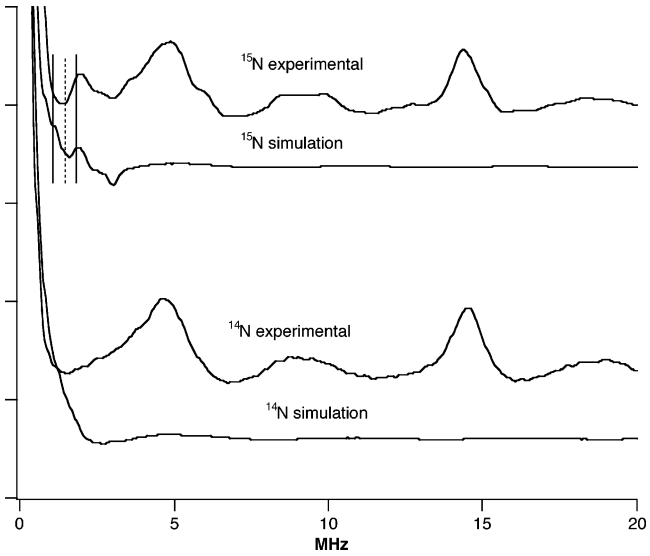

FIGURE 9: Two-pulse ESEEM frequency-domain data and simulations of Cl^--depleted BBY repleted with [^{15}N]azide and [^{14}N]azide. The experimental traces are those of the dotted curves in Figure 8, traces a and b. The pertinent parameters used in the ^{15}N simulation are isotropic coupling constant (A_{iso}) = 0.70 MHz and dipolar coupling constant (A_{dip}) = 0.30 MHz. For the ^{14}N simulation, A_{iso} = 0.50, A_{dip} = 0.21 MHz, nuclear quadrupolar coupling constant eeqQ = 2.0 MHz, and asymmetry parameter η = 0. The simulated time-domain ESEEM spectrum (not shown) is multiplied by an exponential damping function prior to Fourier transformation. The dotted vertical line marks the ^{15}N Larmor frequency, and the solid vertical lines indicate the positions of split peaks centered on the ^{15}N Larmor frequency.

evidence to support a previous suggestion that azide does not significantly interfere with electron transfer between P680 and this acceptor side quinone (*25*).

We note that the Mn S_2 state EPR signal suppression induced by azide on PS II is partly recovered by the addition of bicarbonate (Figure 3). The role, if any, played by bicarbonate in the water splitting chemistry remains unclear. For example, we cannot assert that bicarbonate binding occurs at the ESEEM-detectable azide site reported here. In particular, in parallel work with ^{13}C-labeled bicarbonate, we failed to observe an ESEEM signal from the $I = {}^1/_2$ ^{13}C, suggesting that this site may be remote from the Mn cluster (Yu, Britt, et al., unpublished results). Very recently, it was suggested that chloride participates in establishing a proton relay network by interacting with charged amino acid residues rather than being an integral constituent of the OEC (*32*). In this model, releasing chloride from PS II disrupts the normal proton-relay network and retards the release of protons from the water-splitting reaction. It seems possible that azide displaces bicarbonate from its functional site and delays the advancement from S_1 to S_2 in the presence of chloride. After the removal of Cl^- from the OEC by dialysis, azide may occupy the chloride binding side and bind to the Mn cluster in the OEC. Chloride may act to protect the OEC against inhibition by azide.

It is well-known that, acting as a Lewis base, azide readily binds to transition metals such as manganese (*48*). In this work we observed a weak hyperfine coupling between the S_2 state Mn cluster and the spin $I = {}^1/_2$ ^{15}N of ^{15}N terminally labeled azide, which places this labeled nitrogen within about a 0.5 nm radius of the Mn cluster. The observed azide binding site appears to be competitive with chloride, as the ^{15}N peak was unobservable when the labeled azide was added to an intact BBY preparation in the presence of chloride, or in a chloride-depleted sample where azide and chloride were simultaneously added in the repletion buffer. This is an interesting result, in that it reinforces our earlier ESEEM study with acetate in showing that the chloride binding site is very close to the Mn cluster (*14*). Because of the large quadrupolar interactions, it is difficult to directly observe ENDOR/ESEEM transitions for the two $I = {}^3/_2$ chloride nuclei (^{35}Cl and ^{37}Cl). However, we do observe transitions from ^{2}H-labeled acetate and ^{15}N-labeled azide. Numerous studies have shown that Cl^- is necessary for oxygen evolution (*48*−*51*), but the exact role of chloride in the water oxidation reaction still remains largely unresolved. A new structural model of the OEC does not resolve any Cl^- ions associated with the OEC (*53*). However, our new experiments suggest that azide replaces chloride in a binding site near the Mn cluster, indicating that in the intact OEC chloride is indeed bound close to the manganese cluster, consistent with previous reports and suggestions (*13*, *14*, *27*, *48*−*54*). Further details of the azide binding motif will require more ESEEM and ENDOR studies using a wider range of [^{15}N]azide labels. However, the significant isotropic coupling (0.7 MHz) between the Mn cluster and the terminal azide nitrogen demonstrates an intimate interaction between this anion and the catalytic metal cluster, with direct ligation a very strong possibility.

ACKNOWLEDGMENT

We acknowledge Dr. Jie Wei for helpful discussions.

REFERENCES

1. Britt, R. D. (1996) Oxygen evolution, in *Advances in Photosynthesis: Oxygenic Photosynthesis, The Light Reactions* (Ort, D. R., and Yocum, C. F., Eds.) pp 137−164, Kluwer Academic Publishers, Dordrecht, The Netherlands.

2. Debus, R. J. (1992) The manganese and calcium ions of photosynthetic oxygen evolution, *Biochim. Biophys. Acta 1102*, 269−352.
3. Penner-Hahn, J. E., Fronko, R. M., Pecoraro, V. L., Yocum, C. F., Betts, S. D., and Bowlby, N. R. (1990) Structural characterization of the manganese sites in the photosynthetic oxygen-evolving complex using X-ray absorption spectroscopy, *J. Am. Chem. Soc. 112*, 2549−2557.
4. Riggs-Gelasco, P. J., Mei, R., Ghanotakis, D. F., Yocum, C. F., and Penner-Hahn, J. E. (1996) X-ray absorption spectroscopy of calcium-substituted derivatives of the oxygen-evolving complex of photosytem II, *J. Am. Chem. Soc. 118*, 2400−2410.
5. Cinco, R. M., Robblee, J. H., Rompel, A., Fernandez, C., Yachandra, V. K., Sauer, K., and Klein, M. P. (1998) Strontium EXAFS reveals the proximity of calcium to the manganese cluster of oxygen-evolving photosystem II, *J. Phys. Chem. B 102*, 8248−8256.
6. Latimer, M. J., Derose, V. J., Yachandra, V. K., Sauer, K., and Klein, M. P. (1998) Structural effects of calcium depletion on the manganese cluster of photosystem II: determination by X-ray absorption spectroscopy, *J. Phys. Chem. B 102*, 8257−8265.
7. Sandusky, P. O., and Yocum, C. F. (1984) The chloride requirement for photosynthetic oxygen evolution. Analysis of the effects of chloride and other anions on amine inhibition of the oxygen-evolving complex, *Biochim. Biophys. Acta 766*, 603−611.
8. Brudvig, G. W., Beck, W. F., and De Paula, J. C. (1989) Mechanism of photosynthetic water oxidation, *Annu. Rev. Biophys. Biophys. Chem. 18*, 25−46.
9. Hoganson, C. W., and Babcock, G. T. (1997) A metalloradical mechanism for the generation of oxygen from water in photosynthesis, *Science 277*, 1953−1956.
10. Gilchrist, M. L., Jr., Ball, J. A., Randall, D. W., and Britt, R. D. (1995) Proximity of the manganese cluster of photosystem II to the redox-active tyrosine Y_Z, *Proc. Natl. Acad. Sci. U.S.A. 92*, 9545−9549.
11. Andréasson, L.-E., Vass, I., and Styring, S. (1995) Ca^{2+} depletion modifies the electron transfer on both donor and acceptor sides in photosystem II from spinach, *Biochim. Biophys. Acta 1230*, 155−164.
12. Boussac, A., Zimmermann, J.-L., and Rutherford, A. W. (1989) EPR signals from modified charge accumulation states of the oxygen-evolving enzyme in calcium-deficient photosystem II, *Biochemistry 28*, 8984−8989.
13. Britt, R. D., Peloquin, J. M., and Campbell, K. A. (2000) Pulsed and parallel-polarization EPR characterization of the photosystem II oxygen-evolving complex, *Annu. Rev. Biophys. Biomol. Struct. 29*, 463−495.
14. Clemens, K. L., Force, D. A., and Britt, R. D. (2002) Acetate binding at the photosystem II oxygen evolving complex: an S_2-state multiline signal ESEEM study, *J. Am. Chem. Soc. 124*, 10921−10933.
15. Kühne, H., Szalai, V. A., and Brudvig, G. W. (1999) Competitive binding of acetate and chloride in photosystem II, *Biochemistry 38*, 6604−6613.
16. Hallahan, B. J., Nugent, J. H. A., Warden, J. T., and Evans, M. C. W. (1992) Investigation of the origin of the "S_3" EPR signal from the oxygen-evolving complex of photosystem 2: the role of tyrosine Z, *Biochemistry 31*, 4562−4573.
17. Szalai, V. A., and Brudvig, G. W. (1996) Formation and decay of the S_3 EPR signal species in acetate-inhibited photosystem II, *Biochemistry 35*, 1946−1953.
18. Szalai, V. A., and Brudvig, G. W. (1996) Reversible binding of nitric oxide to tyrosyl radicals in photosystem II. Nitric oxide quenches formation of the S_3 EPR signal species in acetate-inhibited photosystem II, *Biochemistry 35*, 15080−15087.
19. Tang, X.-S., Randall, D. W., Force, D. A., Diner, B. A., and Britt, R. D. (1996) Manganese-tyrosine interaction in the photosystem II oxygen-evolving complex, *J. Am. Chem. Soc. 118*, 7638−7639.
20. Katoh, S. (1972) Inhibitors of electron transport associated with photosystem II in chloroplasts, *Plant Cell Physiol. 13*, 273−286.
21. Stemler, A., and Murphy, J. B. (1985) Bicarbonate-reversible and irreversible inhibition of photosystem II by monovalent anions, *Plant Physiol. 77*, 974−977.
22. Stemler, A., and Jursinic, P. (1983) The effects of carbonic anhydrase inhibitors formate, bicarbonate, acetazolamide, and imidazole on photosystem II in maize chloroplasts, *Arch. Biochem. Biophys. 221*, 227−237.
23. Jursinic, P., and Stemler, A. (1988) Multiple anion effects on photosystem II in chloroplast membranes, *Photosynth. Res. 15*, 41−56.
24. Haddy, A., Hatchell, J. A., Kimel, R. A., and Thomas, R. (1999) Azide as a competitor of chloride in oxygen evolution by photosystem II, *Biochemistry 38*, 6104−6110.
25. Haddy, A., Kimel, R. A., and Thomas, R. (2000) Effects of azide on the S_2 state EPR signals from photosystem II, *Photosynth. Res. 63*, 35−45.
26. Vrettos, J. S., Limburg, J., and Brudvig, G. W. (2001) Mechanism of photosynthetic water oxidation: combining biophysical studies of photosystem II with inorganic model chemistry, *Biochim. Biophys. Acta 1503*, 229−245.
27. Berthold, D. A., Babcock, G. T., and Yocum, C. F. (1981) A highly resolved, oxygen-evolving photosystem II preparation from spinach thylakoid membranes: EPR and electron-transport properties, *FEBS Lett. 134*, 231−234.
28. Ford, R. C., and Evans, M. C. W. (1983) Isolation of a photosystem 2 preparation from higher plants with highly enriched oxygen evolution activity, *FEBS Lett. 160*, 159−164.
29. Campbell, K. A., Gregor, W., Pham, D. P., Peloquin, J. M., Debus, R. J., and Britt, R. D. (1998) The 23 and 17 kDa extrinsic proteins of photosystem II modulate the magnetic properties of the S_1-state manganese cluster, *Biochemistry 37*, 5039−5045.
30. Hui, Y., Jie W., and Carpentier, R. (2000) Degradation of the photosystem I complex during photoinhibition, *Photochem. Photobiol. 72*, 508−512.
31. Arnon, D. I. (1949) Copper enzymes in isolated chloroplasts. Polyphenol oxidase in *Beta vulgaris*, *Plant Physiol. 24*, 1−17.
32. Olesen, K., and Andreasson, L. E. (2003) The function of the chloride ion in photosynthetic oxygen evolution, *Biochemistry 42*, 2025−2035.
33. Sturgeon, B. E., and Britt, R. D. (1992) Sensitive pulsed EPR spectrometer with an 8−18 GHz frequency range, *Rev. Sci. Instrum. 63*, 2187−2192.
34. Mims, W. B. (1984) Elimination of the dead-time artifact in electron spin−echo envelope spectra, *J. Magn. Reson. 59*, 291−306.
35. Britt, R. D., Zimmermann, J.-L., Sauer, K., and Klein, M, P. (1989) Ammonia binds to the catalytic manganese of the oxygen-evolving complex of photosystem II. Evidence by electron spin−echo envelope modulation spectroscopy, *J. Am. Chem. Soc. 111*, 3522−3532.
36. Mims, W. B. (1972) Electron spin−echoes, in *Electron Paramagnetic Resonance* (Geschwind, S., Ed.) pp 263−351, Plenum Press, New York.
37. Mims, W. B. (1972) Envelope modulation in spin−echo experiments, *Phys. Rev. B* 5, 2409−2419.
38. Ghanotakis, D. F., and Yocum, C. F. (1986) Purification and properties of an oxygen-evolving reaction center complex from photosystem II membranes: a simple procedure utilizing a non-ionic detergent and elevated ionic strength, *FEBS Lett. 197*, 244−248.
39. Kawamoto, K., Mano, J., and Asada, K. (1995) Photoproduction of the azidyl radical from the azide anion on the oxidizing side of photosystem II and suppression of photooxidation of tyrosine Z by the azidyl radical, *Plant Cell Physiol. 36*, 1121−1129.
40. De Paula, J. C., Innes, J. B., and Brudvig, G. W. (1985) Electron transfer in photosystem II at cryogenic temperatures, *Biochemistry 24*, 8114−8120.
41. Zimmermann, J. L., and Rutherford, A. W. (1984) EPR studies of the oxygen-evolving enzyme of photosystem II, *Biochim. Biophys. Acta 767*, 160−167.
42. Vermaas, W. F. J., and Rutherford, A. W. (1984) EPR measurements on the effects of bicarbonate and triazine resistance on the acceptor side of photosystem II, *FEBS Lett. 175*, 243−248.
43. Feyziev, Y. M., Yoneda, D., Yoshii, T., Katsuta, N., Kawamori, A., and Watanabe, Y. (2000) Formate-induced inhibition of the water-oxidizing complex of photosystem II studied by EPR, *Biochemistry 39*, 3848−3855.
44. Herbison-Evans, D., and Richards, R. E. (1964) Quadrupole relaxation in nuclear resonance, *Mol. Phys. 7*, 515−526.
45. Forman, R. A. (1966) Nuclear magentic resonance of nitrogen-14 potassium azide, *J. Chem. Phys. 45*, 118−1123.
46. Flanagan, H. L., and Singel., D. J. (1987) Analysis of ^{14}N ESEEM patterns of randomly oriented solids, *J. Chem. Phys. 87*, 5606−5616.
47. Rowan, L. G. (1987) Echo envelope modulation with quadrupole interaction**,** *J. Magn. Reson. 74*, 308−315.

48. Sandusky, P. O., and Yocum, C. F. (1985) The chloride requirement for photosynthetic oxygen evolution. Analysis of the effects of chloride and other anions on amine inhibition of the oxygen-evolving complex, *Biochim. Biophys. Acta 766*, 603−611.
49. Yocum, C. F. (1992) The calcium and chloride requirements for photosynthetic water oxidation, in *Manganese Redox Enzymes* (Pecoraro, V. L., Ed.) pp 71−83, VCH, New York.
50. Wydrzynski, T., Baumgart, F., MacMillan, F., and Renger, G. (1990) Is there a direct chloride cofactor requirement in the oxygen-evolving reactions in photosystem II?, *Photosynth. Res*. *25*, 59−72.
51. Rutherford, A. W., Zimmermann, J.-L., and Boussac, A., (1992) Oxygen evolution, in *The Photosystems: Structure, Function and Molecular Biology* (Barber, J., Ed.) pp 179−229, Elsevier Science Publishers, Amsterdam.
52. Ferreira, K. N., Iverson, T. M., Maghlaoui, K., Barber, J., and Iwata, S. (2004) Architecture of the photosynthetic oxygen-evolving center, *Science 303*, 1831−1838.
53. Britt, R. D., Campbell, K. A., Peloquin, J. M., Gilchrist, L. M., Aznar, C. P., Dicus, M. M., Robblee, J., and Messinger, J. (2004) Recent pulsed EPR studies of the photosystem II oxygen-evolving complex: implications as to water oxidation mechanisms, *Biochim. Biophys. Acta 1655*, 158−171.
54. Peloquin, J. M., Campbell, K. A., Randall, D. W., Evanchik, M. A., Pecoraro, V. L., Armstrong, W. H., and Britt, R. D. (2000) ^{55}Mn ENDOR of the S_2-state multiline EPR signal of photosystem II: implications on the structure of the tetranuclear Mn cluster, *J. Am. Chem. Soc*. *122*, 10926−10942.

BI0505767